Journal of Alloys and Compounds 639 (2015) 470–477

Contents lists available at ScienceDirect

Journal of Alloys and Compounds

journal homepage: www.elsevier.com/locate/jalcom

Synthesis of reduced graphene oxide-iron nanoparticles with superior enzyme-mimetic activity for biosensing application

Lili Li, Chunmei Zeng, Lunhong Ai *, Jing Jiang *

Chemical Synthesis and Pollution Control Key Laboratory of Sichuan Province, College of Chemistry and Chemical Engineering, China West Normal University, Nanchong 637002, PR China

ARTICLE INFO

Article history:
Received 28 January 2015
Received in revised form 19 March 2015
Accepted 22 March 2015
Available online 27 March 2015

Keywords:
Iron nanoparticles
Reduced graphene oxide
Peroxidase-like activity
H_2O_2
Glucose

ABSTRACT

Development of enzyme-mimetic catalysts with sustainability and environmental benignancy has gained considerable attention with the growing demands for large-scale applications in recent years. Here, we demonstrate that the reduced graphene oxide (RGO)-iron nanoparticles (INs) can be utilized as the highly active and cost-effective enzyme-mimetic catalysts for the first time, which have been successfully synthesized by a facile iron-self-catalysis process at room temperature. Benefitting from synergetic effects between RGO and INs, the RGO-INs could efficiently catalyze the oxidization of 3,3′,5,5′-tetramethylbenzidine (TMB) in the presence of H_2O_2 to produce a typical color reaction, showing the much better peroxidase-like activity than that of each individual part. The mechanistic insight into the enhanced peroxidase-like activity of the RGO-INs was investigated systematically. On the basis of the enzyme-mimetic activity of the RGO-INs, the simple, sensitive, selective and cost-effective colorimetric assays for the detection of hydrogen peroxide and glucose with naked eyes were successfully established. The RGO-INs showed several prominent advantages, such as facile preparation, low cost, tunability in catalytic activity, and low detection limit, over natural peroxidase or other nanomaterial-based alternatives, holding great potential as enzymatic mimics for biosensing applications.

1. Introduction

Natural enzymes are well-known class of biological catalysts with high substrate specificities and high activity under mild reaction conditions, which have found significant and widespread applications in medicine, chemical industry, food processing and agriculture [1,2]. However, they intrinsically own some drawbacks, including limited natural sources, inherent instability, and requiring expensive and time-consuming purification, restricting their practical applications greatly. To overcome these limitations of natural enzymes while maintain the high reactivity, numerous efforts have been focused on the design and construction of artificial enzymes that can mimic the complexities and functions of natural enzymes. Particularly, the merging of nanotechnology with biology has ignited research interest for designing and seeking functional nanomaterials mimicking catalytically active enzymes [3,4]. For instance, inorganic metal oxides (Fe_3O_4 [5], MnO_2 [6], Co_3O_4 [7], CuO [8], TiO_2 [9], V_2O_5 [10]), metal sulfides (CuS [11], FeS [12], CdS [13], MoS_2 [4]) and carbon (carbon nanodots [14], graphene oxide [15], carbon nanotube [16]) nanomaterials have been discovered to possess intrinsic peroxidase-like activity and shown promising potential in environmental remediation [17] and biosensing applications. Meanwhile, noble metal nanoparticles have been emerging as another type of the most promising materials with excellent peroxidase-mimetic activity because of their unique physical and chemical properties. For example, Au [18], Pt [19], Ag [20] nanoparticles have been reported separately to possess an intrinsic peroxidase-like activity. Their nanostructured alloys such as Au@Pt [21], AgM (M = Au, Pd, Pt) [22], Au@PtAg [23], and AuPd [24] achieve excellent ability toward peroxidase mimicry for catalytic acceleration of specific reaction as well. However, their practical large-scale applications are restricted dramatically by the inevitable disadvantages of high price and scarcity. Towards this end, it is of considerable interest and great significance to develop cheap and earth-abundant alternatives to noble metal catalyst to achieve high efficiency at low cost.

Iron is an earth abundant metal, and its oxides have been demonstrated as highly active peroxidase mimetics [25,26]. Apparently, utilization of metallic iron as peroxidase mimetics for biosensing application is remarkably attractive because of the anticipated sustainability and environmental benignancy. Very recently, Huang and his coworkers have been demonstrated a non-noble metal-based bimetallic Fe–Co nanoparticles indeed

* Corresponding authors. Tel./fax: +86 817 2568081.
E-mail addresses: ah_aihong@163.com (L. Ai), 0826zjjh@163.com (J. Jiang).

http://dx.doi.org/10.1016/j.jallcom.2015.03.176
0925-8388/

possesses peroxidase-like activity which exhibits high affinity to H_2O_2 and found that the combination with metallic cobalt generates the synergistic effect to enhance the peroxidase-like activity of monometallic iron [27]. However, to a certain extent, it is still not fully understood or very limitedly what dominates the catalytic mechanism and how metallic iron interacts with substrates during biosensing application. More surprisingly, to the best of our knowledge, there are no reports in the literature on the peroxidase mimicking behaviors of other metallic iron-based nanoparticles.

To maximize the reactivity and stability of metal NPs, a robust support is usually required to protect them against dissolution and aggregation. Owing to its large specific surface area, great mechanical strength, and low manufacturing cost, graphene has been considered a promising candidate as a new two-dimensional (2D) carrier to support metal nanoparticles [28,29]. Moreover, graphene-family materials represent the interesting properties which would be favorable for the design of nanomaterial-based enzyme mimics [30]. The opened surface areas of graphene are readily accessible to substrates with a small diffusion and transport barrier, while its rich surface chemistry ensures the stability of the supported systems. Thus, it is reasonably expected that graphene would be an effective 2D carrier for loading metal nanoparticles to create highly active enzyme mimetics and to further realize the cooperatively enhanced performances by the combination of the respective properties of each component.

Bearing these issues in mind, we herein report a facile and rational synthesis of reduced graphene oxide-iron nanoparticles (RGO-INs) by an iron-self-catalysis process and demonstrate the resulting RGO-INs can be utilized as the highly active and cost-effective enzyme-mimetic catalysts for the first time. The synthetic strategy is simple, inexpensive and scalable, and the whole processing is completely at room temperature. Benefitting from synergetic effects between INs and RGO, the RGO-INs could catalyze the oxidation of different peroxidase substrates in the presence of H_2O_2 to produce typical color reactions, which showed the better peroxidase-like activity than that of each individual part. Based on the peroxidase-like behavior of the RGO-INs, the simple, sensitive, selective and cost-effective colorimetric assays for the detection of H_2O_2 and glucose with naked eyes were successfully established.

2. Experimental

2.1. Materials

Graphite powder, $KMnO_4$, $NaNO_3$, H_2SO_4 (98%), $FeCl_3{\cdot}6H_2O$, $NaBH_4$, acetic acid (HAc), sodium acetate (NaAc) and H_2O_2 (30 wt%) were purchased from Kelong Chemical Reagents Company (Chengdu, China). Na_2HPO_4, KH_2PO_4, polyvinylpyrrolidone (PVP) and 3,3′,5,5′-tetramethylbenzidine dihydrochloride (TMB) were purchased from Aladin Ltd (Shanghai, China). Glucose, fructose, lactose, maltose, and glucose oxidase (GOx, 340 U mg^{-1}) were purchased from Sangon Biochemical Engineering Technology Co., Ltd (Shanghai, China). All chemicals used in this study were analytical reagent grade. Freshly deionized water was used to prepare all solutions and conduct all of the tests. Graphite oxide was synthesized from oxidation of nature graphite powder by a modified Hummers method.

2.2. Preparation of reduced graphene oxide-iron nanoparticles (RGO-INs)

The preparation procedure for the RGO-INs was schematically illustrated in Fig. 1. In a typical synthesis, the required amount of graphite oxide was dispersed in deionized water by ultrasonication for 1 h. 5 mL of aqueous solution containing $FeCl_3{\cdot}6H_2O$ (0.6757 g) and PVP (0.111 g) was poured into GO solution and sonicated for another one hour. Afterward, 20 mL of $NaBH_4$ (1.25 g) solution was added dropwise into the above mixture solution under constant stirring at room temperature. After the reaction of 3 h, the black solid was collected by filtration, washed with ethanol several times, and dried in flowing nitrogen. The catalysts with different ratios of RGO to INs for the designed RGO-INs were listed in Table S1 (see Supporting Information). Among all the samples, the RGO-INs-5% showed the best peroxidase-like activity; therefore, if no further notification is provided, the RGO-INs notation in this study refers to RGO-INs-5%.

2.3. Characterization

The powder X-ray diffraction (XRD) measurements were recorded on a Rigaku Dmax/Ultima IV diffractometer with monochromatized Cu Kα radiation (λ = 0.15418 nm). The morphology was observed with a JEOL JSM-6510LV scanning electron microscope (SEM) and transmission electron microscope (TEM, FEI Tecnai G20). The elemental composition of the samples were characterized by energy-dispersive X-ray spectroscopy (EDS, Oxford instruments X-Max). The Fourier transform infrared (FTIR) spectrum was measured on a Nicolet 6700 FTIR spectrometric Analyzer using KBr pellets. Raman measurements were carried out by a confocal laser micro-Raman spectrometer (Thermo DXR Microscope, USA). The laser was 633 nm with a 5 mW.

2.4. Peroxidase-like catalytic activity of the RGO-INs

To evaluate the peroxidase-like catalytic activity of the RGO-INs, the catalytic oxidation of the peroxidase substrate TMB in the presence of H_2O_2 was tested. The measurements were carried out by monitoring the absorbance change of TMB at 652 nm. In a typical experiment, 80 μL of the RGO-INs dispersion (1 mg mL^{-1}) was mixed in 1600 μL of NaAc buffer solution (pH 3.0), followed by adding 400 μL of TMB solution (1 mM, ethanol solution). Then, 20 μL of H_2O_2 with various concentrations was added into the mixture. The mixed solution was incubated at 40 °C for 30 min. For comparison, the control experiments were also conducted under the same conditions by using bare RGO, INs or their physical mixture as catalysts. In addition, the influences of reaction buffer pH and incubation temperature on the peroxidase-like catalytic activity of the RGO-INs were also investigated.

2.5. Bioassay

Kinetic measurements were carried out in time course mode by monitoring the absorbance change at 652 nm. To investigate the mechanism, assays were carried out by varying concentrations of TMB at a fixed concentration of H_2O_2 or vice versa. Experiments were performed using 38 μg mL^{-1} RGO-INs in 1600 μL of reaction buffer (0.2 M NaAc, pH 3.0) with 0.09 mM TMB as substrate, or 0.47 mM H_2O_2, unless otherwise stated. The apparent kinetic parameters were calculated using Lineweaver–Burk plots of the double reciprocal of the Michaelis–Menten equation: $1/v = K_m/V_{max}(1/[S] + 1/K_m)$, where v is the initial velocity, V_{max} is the maximal reaction velocity, $[S]$ is the concentration of substrate, K_m is the Michaelis constant [14,31].

2.6. Detection of glucose using the RGO-INs as peroxidase-like mimetics

Glucose detection was carried out as follows: firstly, 100 μL of GOx aqueous solution (1.0 mg mL^{-1}) and 100 μL of D-glucose with various concentration were mixed in 500 μL of NaH_2PO_4 buffer (0.5 mM, pH 7.0) and incubated at 37 °C for 1 h; then 200 μL of TMB (5 mM, ethanol solution), 100 μL of the RGO-INs stock solution (1 mg mL^{-1}) and 4.00 mL of NaAc buffer (0.2 M, pH 3.0) were successively added to the glucose reaction solution; finally, the mixed solution was incubated at 40 °C for 30 min for standard curve measurement.

3. Results and discussion

Our synthesis strategy was based on the *in situ* simultaneous reduction of Fe^{3+} and GO at room temperature. Graphite oxide with abundant oxygenous groups was highly negatively charged, which was firstly liquid exfoliated by ultrasonication to form a stable aqueous solution. When Fe^{3+} ions were introduced, the electrostatic interactions between positively charged Fe^{3+} and GO provided a necessary driving force for the effective enrichment of Fe^{3+} onto GO. During the chemical reduction process, iron nanoparticles (INs) were then *in situ* formed on the surface of the reduced GO. Importantly, reduction of GO in our case can be achieved in a mild condition (e.g. room temperature and short reaction time). As previously reported, the reactive hydrogen atoms released from the $NaBH_4$ hydrolysis can reduce the oxygenous groups on the GO, which is a critical step toward the chemical reduction ability of $NaBH_4$ [32]. It is believed that *in situ* formed INs can act as the catalyst to accelerate the $NaBH_4$ hydrolysis to release active hydrogen. To support this hypothesis, we further monitored the amounts of hydrogen generation during the synthesis process (Fig. 2). It is interestingly found that GO was incapable for hydrogen generation, while both the INs and RGO-INs could induce *in situ* fast hydrogen generation, confirming that the formation of

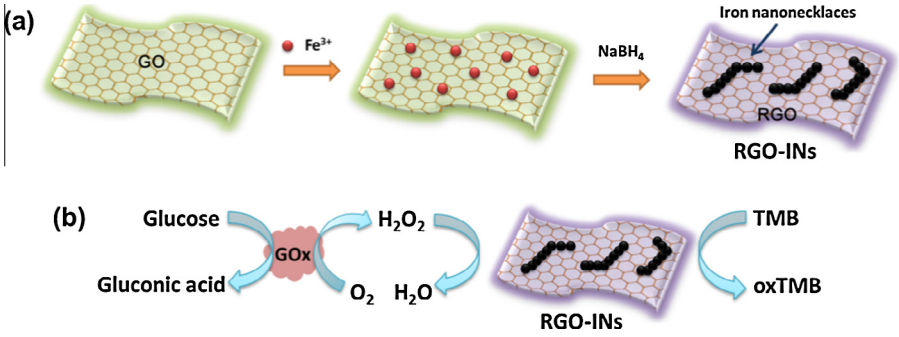

Fig. 1. Schematic diagrams of (a) the synthesis process of the RGO-INs and (b) colorimetric detection of glucose using the RGO-INs as peroxidase-like mimetics.

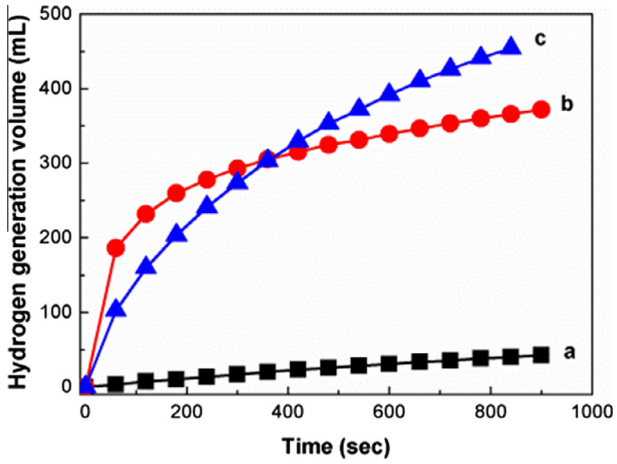

Fig. 2. Hydrogen generation during the sample synthesis process at room temperature: (a) GO, (b) INs and (c) RGO-INs.

the RGO-INs at room temperature had undergone an iron-self-catalysis reduction process.

Fig. 3a shows a typical SEM image of the RGO-INs. The iron nanoparticles present the nanonecklace-like morphology formed through connection of nanospheres one by one, looking like "pearl necklaces". The diameters of these nanoparticles were in the range of 20–50 nm. Meanwhile, they were effectively decorated on the surface of graphene nanolayers. It should be noted that the graphene nanolayers hybridized randomly with nanoparticles endow them with good connection and intimate contact, which is beneficial to the subsequent catalysis applications. The detailed morphology of the RGO-INs was further investigated by transition electron microscopy (TEM). Fig. 3b shows a typical TEM image of the RGO-INs, which further confirms the structure characteristic of nanonecklace-like iron and crumpled silk-like morphology of graphene. The nanonecklaces had diameters of 20–50 nm and lengths of several micrometers and were well distributed onto the surface of the flexible graphene nanolayers. Moreover, no free nanoparticles were found outside of the graphene nanolayers during the TEM observation, indicating a perfect combination between the RGO and the INs. The HRTEM image (Fig. 3c) of the RGO-INs further revealed that the core–shell structure of INs, which can be ascribed to the surface iron combined with oxygen of atmosphere to form oxide layers during the catalyst preparation and storage process, consistent with previous reports [33–35].

Fig. S1 shows the XRD patterns of the GO, bare INs and RGO-INs. In the XRD pattern of GO, a sharp and intense diffraction peak was observed at $2\theta = 10.3°$, which is associated with the interplanar spacing of GO sheets, corresponding to the characteristic (001) reflection of GO. The RGO-INs exhibit face-centered cubic (fcc) Fe^0 phase (JCPDS no. 88-2324) similar to the pure INPs, where a broad characteristic diffraction peak centered at $2\theta = 44.9°$ was observed. In addition, the disappearance of the peak at $2\theta = 10.3°$ confirms that the graphite oxide has been exfoliated to GO and some oxygen-containing groups in GO have been removed during the chemical reduction process. The composition of the RGO-INs was determined by X-ray energy-dispersive spectroscopy (EDS), as shown in Fig. S2, which unambiguously demonstrates the coexistence of Fe, O and C elements in the product. The oxygen element could come from the residual oxygen-containing functional groups on RGO and the oxide layer of INPs. Fig. 4a shows the FTIR spectra of GO and RGO-INs. The characteristic absorption peaks of GO were observed at 3439 cm^{-1} (the O—H stretching mode), 1730 cm^{-1} (the C=O stretching mode), 1630 cm^{-1} (the C=C stretching mode), 1389 cm^{-1} (the C—OH stretching mode), and 1068 cm^{-1} (the C—O—C stretching mode) [36,37]. It can be seen clearly that the disappearance of C=O peak and the remarkable decrease in intensity of C—OH and C—O—C peak for GO in the spectrum of

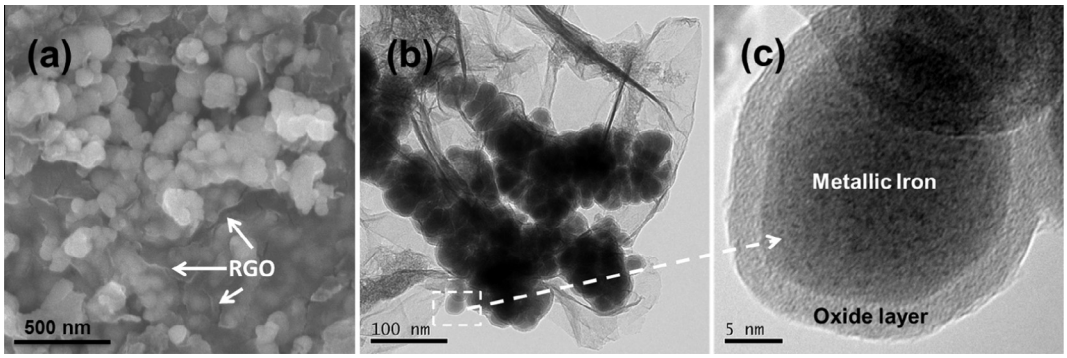

Fig. 3. SEM (a), TEM (b) and HRTEM (c) images of the RGO-INs.

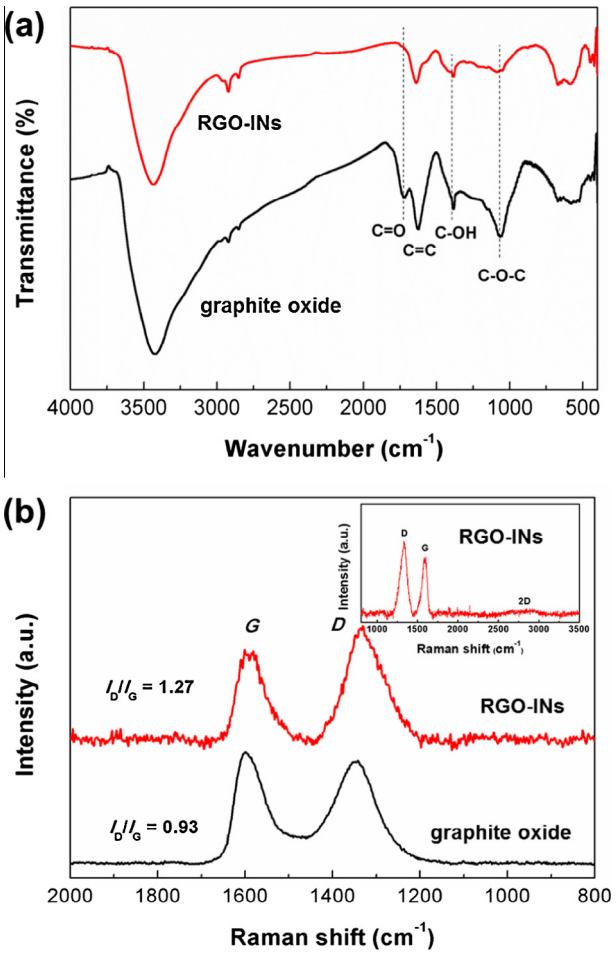

Fig. 4. FTIR (a) and Raman spectra (b) of the GO and RGO-INs.

the RGO-INs, indicating most of oxygen-containing functional groups in the GO have been removed. Fig. 4b shows the Raman spectra of GO and RGO-INs. For the GO, two prominent bands at around 1350 and 1590 cm^{-1} can be observed, corresponding to the local defects or disorder atomic arrangement of sp^3-carbon (D-band) and the plane vibration of the sp^2-carbon in the two-dimensional lattice (G-band), respectively [38]. In comparison with GO (I_D/I_G = 0.93), it is evident that RGO-INs displays the increased intensity ratio of the D- to G-band (I_D/I_G = 1.27), confirming the efficient reduction of GO during *in situ* preparation process [39]. In addition, the 2D band at around 2700 cm^{-1} is the overtone of the D band, originated from two phonon double resonance, which is sensitive to the number of graphene layers [40–44]. A weak and broad 2D band in RGO-INs (inset), which is an indication of disorder and coupling of the stacked multilayers of graphene sheets.

The detailed chemical and electronic states of the RGO-INs were determined by X-ray photoelectron spectroscopy (XPS). Fig. 5 shows the XPS survey spectrum and high-resolution XPS spectra of the RGO-INs. The XPS survey spectrum (Fig. 5a) demonstrates that C, O, and Fe elements existed in the RGO-INs. Fig. 5b shows the high-resolution XPS spectra of Fe2p. The binding energies of 711.6 and 725.3 eV with a satellite signal at 718.8 eV are characteristic of Fe^{3+} in Fe_2O_3; while a weak peak at a low binding energy of 706.0 eV is typical for pure iron [35,45]. Considering the XPS could only detect the photoelectrons from the outer surface of 10 nm, the thickness of the Fe_2O_3 shell in the nanoparticles should be less than 10 nm because the metallic iron signal was detected, consistent with TEM observation. The high-resolution XPS spectrum of the O 1s could be fitted by four peaks (Fig. 5c), which are attributed to the oxygen components on the RGO (OH, C—O: 531.9 eV, C═O: 533.0 eV, and O—C═O: 534.0 eV) [46] and the Fe—O bonds (530.8 eV) of Fe_2O_3 [45], respectively. Fig. 5d shows the high-resolution XPS spectrum of the C 1s, which can be deconvoluted into three surface components, corresponding to the C—C (284.6 eV), C—O (286.0 eV) and O—C═O (289.5 eV) carbon components on the RGO [47]. This result reveals that the graphene in the RGO-INs has a very high degree of reduction.

The peroxidase-like activities of the as-prepared RGO-INs were evaluated by the catalytic oxidation of a typical peroxidase substrate 3,3′,5,5′-tetramethylbenzidine (TMB) that could generate a blue color reaction in the presence of H_2O_2. As shown in Fig. 6A, the RGO-INs present a remarkable catalytic activity toward the oxidation of TMB substrate in the presence of H_2O_2, which can develop a typical blue-green color with an intense characteristic absorbance at 652 nm (curve e). In contrast, the RGO-INs (curve c) or H_2O_2 (curve d) alone was incapable to produce a significant change of the solution color, as compared to that of the blank solution containing only TMB (curve a). To further confirm the characteristic peroxidase-like activity of the RGO-INs, other typical peroxidase substrates such as o-phenylenediamine (OPD) and 1,2,3-trihydroxybenzene (THB) were employed as replacements for the TMB to proceed the identical catalytic reaction. As shown in Fig. S3 (see Supporting Information), the RGO-INs can also catalyze the OPD and THB to produce the typical color reactions in the presence of H_2O_2. All these observations suggest that the RGO-INs possess excellent peroxidase-like catalytic activity. Noticeably, the previously reported results have shown that the leaching solution from the catalysts could affect the catalytic activity [31,48]. In order to rule out the possibility that the observed catalytic activity results from the RGO-INs rather than from the free leaching ions, we further performed a leaching experiment. The RGO-INs was incubated in the reaction buffer (pH 3.0) for 2 h and then centrifuged to collect the supernatant. The leaching solution was then tested towards the TMB oxidation reaction (Fig. 6B). Evidently, the leaching solution had no catalytic activity, confirming that the observed peroxidase-like activity was due to intact RGO-INs. In addition, we further compared the catalytic activity of the RGO-INs under aerobic and anaerobic conditions (Fig. 6C). It is clear that both conditions show the comparable absorbance at 652 nm, indicating that the activity of the RGO-INs could not be affected by the molecular oxygen in air.

Similar to other NPs-based peroxidase mimetics and HRP, the catalytic activity of the RGO-INs depends on pH, temperature, and H_2O_2 concentration. The peroxidase-like activity of RGO-INs was measured by varying the pH from 2 to 12, the temperatures from 20 °C to 70 °C, the H_2O_2 concentration from 0.095 μM to 545 mM. Under our experimental conditions, the optimal pH and temperature were 3.0, 40 °C and 10 mM H_2O_2, respectively (Fig. S4 in the Supporting Information). Based on the above results, RGO-INs-based H_2O_2 detection can be carried out in a relatively wide range of H_2O_2 concentration.

The peroxidase-like catalytic activity of the RGO-INs is further compared with pure RGO and free INs. Fig. S5 shows the UV–vis spectra of the TMB-H_2O_2 system catalyzed by different catalysts. As can be seen, pure RGO did not produce an apparent change of the solution color, indicating its limited peroxidase-like catalytic activity; while free INs could generate considerable colorimetric responses, revealing the intrinsic peroxidase-like catalytic activity of metallic iron. Interestingly, after *in situ* combination with RGO, the RGO-INs became more active, which lead to the absorbance at 652 nm significantly higher than that of free INs. To insight into the positive effect in the RGO-INs system, we further quantitatively compare the absorbance values at 652 nm in the presence of different catalysts, as shown in Fig. 6D. Obviously, the RGO-INs were

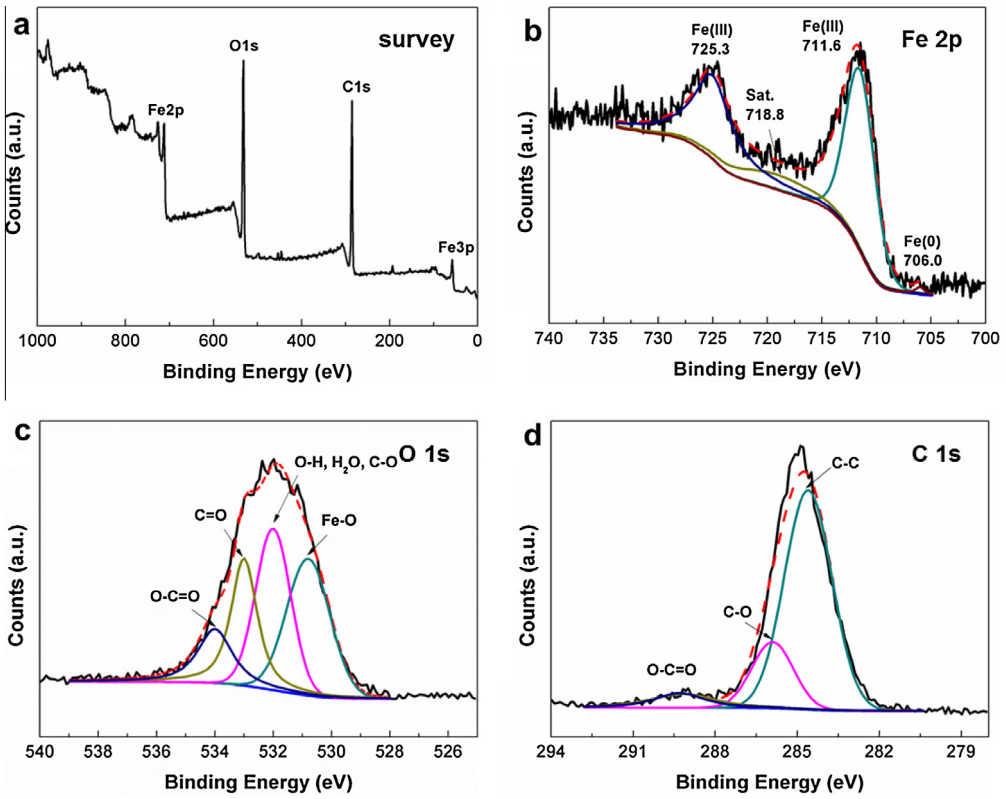

Fig. 5. XPS spectra of RGO-INs: (a) survey, (b) Fe 2p, (c) O 1s and (d) C 1s.

more catalytically active than the pure RGO and free INs, which were about 6.3 times as high as that of pure RGO, 3.3 times that of free INs, and even 2.2 times higher than the sum of the absorbance value of the RGO and INs. Furthermore, we carried out a control experiment on the physical mixture of RGO with INs (RGO/INs) and found that their physical mixture showed much weaker catalytic activity than the RGO-INs. These results imply the favorable synergistic effect existed in RGO-INs system. In addition, the peroxidase-like activity of the RGO-INs depends closely on the content of RGO. Among all the RGO-INs samples, the optimal catalyst was found to be RGO-INs-5% (Fig. S6 in the Supporting Information), which may be benefited from the favorable dispersibility of INs on RGO and the synergistically effective interaction between RGO and INs.

To gain insight into how the RGO interacts with INs to achieve the synergistic catalysis in the RGO-INs, electrochemical evaluation of the RGO-INs was investigated by the electrochemical impedance spectroscopy (EIS). Fig. S7 shows EIS Nyquist plots of free INs and RGO-INs in 0.1 M KCl containing 5 mM $[Fe(CN)_6]^{4-/3-}$ (see Supporting Information). It is known that EIS measurement can be used to determine the charge-transfer resistance as indicated by the diameter of the preceding semicircle in Nyquist plot. Normally, the smaller radius means the better ability to transfer charge. In comparison with free INs, the decreased radius of the Nyquist arc of RGO-INs was observed, reflecting that the introduced RGO is benefit to the improvement of charge transfer efficiency in INs due to its excellent electrical conductivity.

To further investigate the mechanism of the peroxidase-like catalytic activity of the RGO-INs, we further carried out the steady-state kinetic assays by changing one substrate concentration while keeping the other substrate concentration constant. As shown in Figs. S8a and S8b, in a certain range of substrate concentrations, typical Michaelis–Menten curves were obtained for H_2O_2 or TMB, respectively. The maximum initial velocity (V_{max}) and Michaelis–Menten constant (K_m) were obtained from the Lineweaver–Burk plots and listed in Table S2 (see Supporting Information). K_m is generally identified as an indicator of binding affinity of the enzyme to the substrates and can be applied similarly here to determine enzyme mimic-substrate interaction. The lower value of K_m represents stronger affinity between the enzyme (catalysts) and substrate (TMB or H_2O_2). The apparent K_m of the RGO-INs with H_2O_2 as the substrate was much higher than that of HRP, which is in agreement with the previous observations that a higher H_2O_2 concentration was required to obtain maximal activity for the RGO-INs [49,30]. The K_m value of the RGO-INs with TMB as substrate is remarkably lower than that of HRP (Table S2 in the Supporting Information), suggesting that the RGO-INs have a larger affinity for TMB than HRP. This may be attributed to synergistic effects in the RGO-INs system, resulting from the excellent ability of RGO toward the adsorption and enrichment of TMB, which is critical to the subsequent interfacial charge transfer process. Additionally, we measured their activity toward TMB and H_2O_2 with various concentrations, respectively. Figs. S8c and S8d show the double reciprocal plots of initial velocity against one substrate concentration obtained over a range of the second substrate concentrations, which reveal the characteristic parallel lines of a ping-pong mechanism were characterized with parallel lines, similar to HPR [25,50]. The experimental facts indicate that the RGO-INs bind and react with the first substrate and then release the first product before reacting with the second substrate.

In light of the above results, we would like to discuss the enhanced peroxidase-like catalytic activity of the RGO-INs. Since neither H_2O_2 nor RGO-INs can effectively oxidize TMB, the interactions between RGO-INs and H_2O_2 and TMB are critical for the catalytic reaction. The negligible change observed in aerobic and anaerobic reactions (Fig. 6C) reveal the molecular oxygen in air plays minor role in the peroxidase-like catalytic process. Similar to previous observations [33–35], iron oxide was easily generated

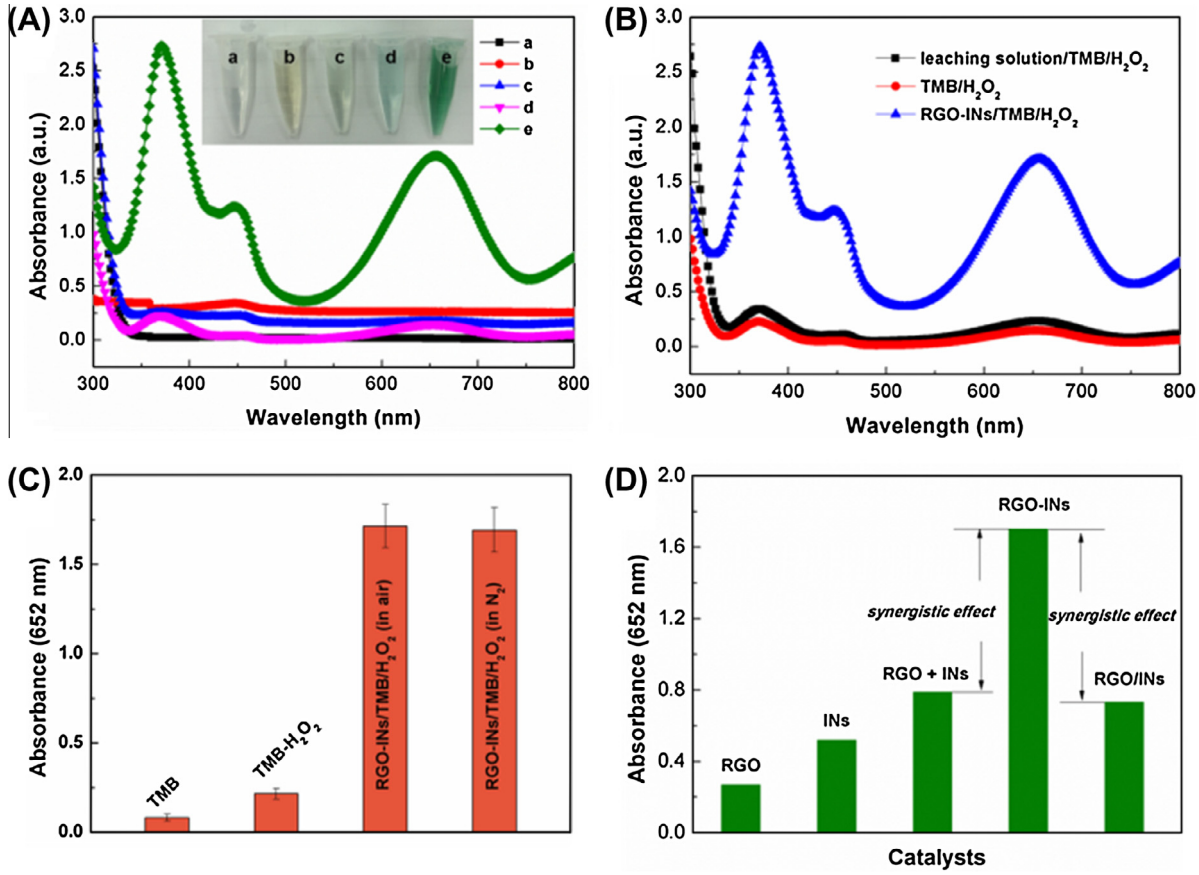

Fig. 6. (A) UV–vis spectra and corresponding photographs (inset) of different reaction systems: TMB solution (a), H_2O_2/RGO-INs (b), TMB/RGO-INs (c), TMB/H_2O_2 (d), and TMB/H_2O_2/RGO-INs (e) in acetate buffer (pH 3.0). ([TMB]: 0.19 mM; [H_2O_2]: 10 mM; [RGO-INs]: 38 μg mL^{-1}). (B) UV–vis spectra of the TMB oxidation system in the presence of the leaching solution and the RGO-INs. (C) UV–vis absorbance at 652 nm of the TMB oxidation system in the presence of the RGO-INs in air and nitrogen. (D) Quantitative comparison of the catalytic activity of different catalysts.

and grown on the surface of iron nanoparticles when freshly prepared iron nanoparticles were exposed to water, resulting in the formation of core–shell structure. Furthermore, no observation on the peroxidase-like catalytic activity of the leaching solution solidly confirms the tightly bound iron ions in the RGO-INs. Based on above consideration, we think the *in situ* formed oxide shell could guide the effective iron cycling and simultaneously produce the highly reactive hydroxyl radicals (·OH) to initiate peroxidase-like catalytic reaction, which is indispensable for the excellent activity of the RGO-INs. As schematically illustrated in Fig. 7, the *in situ* formation of surface bound ferrous ions is thermodynamically favored by electron transfer from INs core to the surface of oxide layer ($2Fe^{III} + Fe^0 \rightarrow 2Fe^{II}$, $\Delta E = 1.21$ eV) [51,52], which would react with H_2O_2 to produce ·OH with strong oxidative ability under acidic pH conditions ($Fe^{II} + H_2O_2 \rightarrow Fe^{III} + {\cdot}OH + OH^-$), thus offering effective transmission pathway of electrons via surface Fe^{III}–Fe^{II} switch for the sustained production of ·OH. On the other hand, the alternative electron transfer from INs to the RGO nanosheets via the conduction band of the iron oxide shell to reduce H_2O_2 could be spontaneously driven by the Ohmic contact between INs and iron oxide shell, because the work function of Fe^0 (4.5 eV) is lower than that of iron oxide (5.6 eV) [45]. To validate these assumptions, we used XPS analysis to characterize Fe species in RGO-INs before and after peroxidase-like catalytic reaction (Fig. S9 in the Supporting Information). It is clear that the amount of Fe^{III} is decreased while the proportion of Fe^{II} is significantly increased after catalytic reaction, which infers that Fe^{III} and Fe^{II} can mutually transform one into another during the catalytic reaction, indicating the possible surface Fe^{III}–Fe^{II} switch. We also employ the well-established fluorescence method to determine ·OH radicals in the catalytic system (Fig. S10a). It is clear that the significant change in fluorescent intensity at 425 nm was

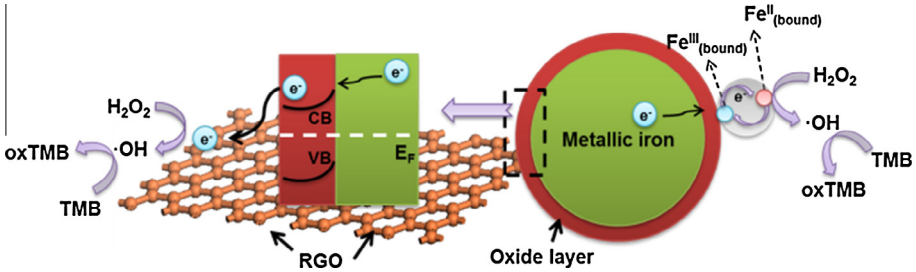

Fig. 7. A schematic diagram to illustrate the enhanced peroxidase-like catalytic activity of the RGO-INs.

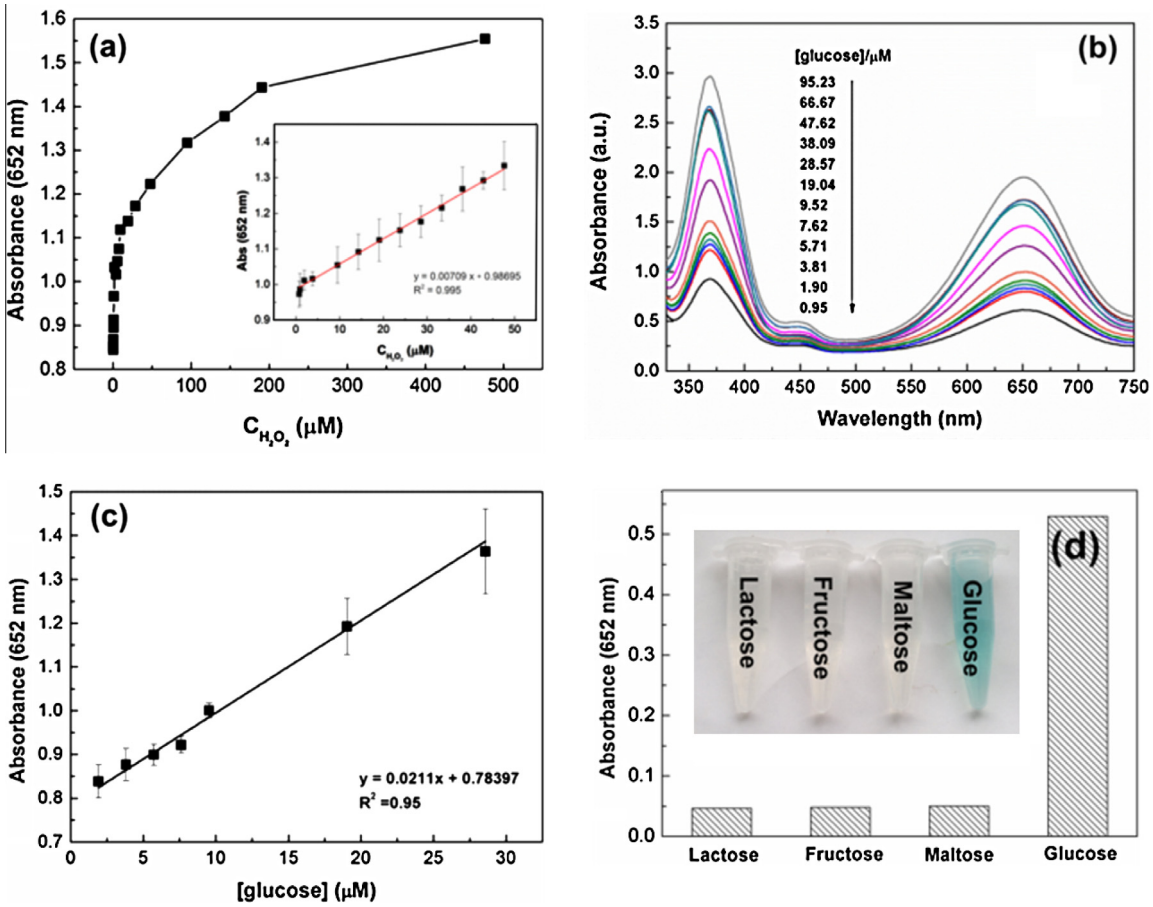

Fig. 8. (a) A dose–response curve for H_2O_2 detection using the RGO-INs under the optimum conditions (inset: linear calibration plot for H_2O_2 detection). (b) UV–vis absorption spectra of oxidazed TMB using the RGO-INs under the optimum conditions for glucose detection. (c) Linear calibration plot for glucose detection. (d) Selectivity analysis for glucose detection by monitoring the relative absorbance. The analyte concentrations were as follows: 1 mM lactose, 1 mM fructose, 1 mM maltose and 100 μM glucose. Inset: the color change of different solutions. (For interpretation of the references to colour in this figure legend, the reader is referred to the web version of this article.)

observed for RGO-INs/H_2O_2 system, indicating the effective generation of ·OH radicals. Noticeably, no observable PL intensity was detected in the absence of the RGO-INs. This solidly confirms that the RGO-INs can catalytically activate H_2O_2 to produce ·OH radicals that could react with TMB to produce the color reaction. To further support this mechanism, the electrocatalytic activity of the RGO-INs modified glassy carbon electrodes (RGO-INs/GCE) towards the electrochemical reduction of H_2O_2 was studied by using their amperometric response. The reduction current increased sharply to a steady-state value for the RGO-INs/GCE upon the addition of an aliquot of H_2O_2 (Fig. S10b in the Supporting Information), which shows a notably better response to H_2O_2 than the individual INs and RGO. Based on the above results, it is believed that the peroxidase-like activity of the RGO-INs could originate from its catalytic activation of H_2O_2 through electron transfer to produce ·OH radicals by an iron-recycling process.

Taking into account to the aforementioned peroxidase-like activity of the RGO-INs, we therefore developed a simple colorimetric method for detection of H_2O_2 based on RGO-INs-catalyzed color reaction. Fig. 8a shows a typical H_2O_2 concentration–response curve for the RGO-INs, where the H_2O_2 can be detected in a linear range from 0.76 to 47 μM (R^2 = 0.995). The detection limit is estimated to be 0.2 μM, which is much lower than that of previously reported nanomaterials-based peroxidase mimics (Table S3 in the Supporting Information). Considering that GOx can specifically catalyze the glucose oxidation in the presence of oxygen to produce H_2O_2, the proposed colorimetric method could be extended for the sensitive detection of glucose by coupling with GOx. Fig. 8b and c shows typical absorption profiles and concentration–response curve for glucose detection. Under the optimized condition, a linear relationship was achieved between the absorbance and the glucose concentration in the range of 2.0–30 μM (R^2 = 0.995), with a very low detection limit of 0.8 μM, showing the higher sensitivity than those of previously reported nanomaterials-based peroxidase mimics (Table S3 in the Supporting Information). To test the selectivity of the RGO-INs-based colorimetric assay for glucose, control experiments were carried out using lactose, fructose, and maltose. The selectivity of the colorimetric method was shown in Fig. 8d. The absorbance at 652 nm of oxidized TMB with glucose is obviously higher than the glucose analogs, although the concentrations of these analogs are about 10-fold higher than that of glucose. The signals of glucose analogs are as low as that of the glucose, and the color difference can be observed by the naked eye (inset in Fig. 8d). Thus, the colorimetric method developed here showed high sensitivity and selectivity towards glucose.

4. Conclusions

In summary, we have reported the iron-self-catalysis method for the synthesis of iron nanoparticles anchored *in situ* on reduced graphene oxide (RGO-INs) under mild condition. The newly synthesized RGO-INs can catalyze the oxidization of typical peroxidase

substrates such as TMB, OPD and THB by H_2O_2 to produce a typical color reaction. The RGO-INs possesses much better intrinsic peroxidase-like activity than that of each individual part and its catalysis is strongly dependent on pH, temperature and H_2O_2 concentration, similar to HRP. The mechanistic insight into the enhanced peroxidase-like activity of the RGO-INs was proposed. As a novel peroxidase mimic, the RGO-INs provide a simple, inexpensive, highly sensitive and selective colorimetric assay to detect H_2O_2 and glucose. The RGO-INs showed several prominent advantages, such as ease of preparation, low-cost, high activity, and low detection limit, holding great potential for applications in biotechnology.

Acknowledgements

This work was supported by the National Natural Science Foundation of China (21207108), the Sichuan Youth Science and Technology Foundation (2013JQ0012), and the Research Foundation of CWNU (12B018, 14E016).

Appendix A. Supplementary material

Supplementary data associated with this article can be found, in the online version, at http://dx.doi.org/10.1016/j.jallcom.2015.03.176.

References

[1] Y. Lin, J. Ren, X. Qu, Adv. Mater. 26 (2014) 4200–4217.
[2] Y. Lin, A. Zhao, Y. Tao, J. Ren, X. Qu, J. Am. Chem. Soc. 135 (2013) 4207–4210.
[3] H. Wei, E.K. Wang, Chem. Soc. Rev. 42 (2013) 6060–6093.
[4] Y. Lin, J. Ren, X. Qu, Acc. Chem. Res. 47 (2014) 1097–1105.
[5] H. Wei, E.K. Wang, Anal. Chem. 80 (2008) 2250–2254.
[6] X. Liu, Q. Wang, H. Zhao, L. Zhang, Y. Su, Y. Lv, Analyst 137 (2012) 4552–4558.
[7] J. Mu, Y. Wang, M. Zhao, L. Zhang, Chem. Commun. 48 (2012) 2540–2542.
[8] W. Chen, J. Chen, Y.-B. Feng, L. Hong, Q.-Y. Chen, L.-F. Wu, X.-H. Lin, X.-H. Xia, Analyst 137 (2012) 1706–1712.
[9] L. Zhang, L. Han, P. Hu, L. Wang, S. Dong, Chem. Commun. 49 (2013) 10480–10482.
[10] R. Andre, F. Natalio, M. Humanes, J. Leppin, K. Heinze, R. Wever, H.-C. Schroder, W.E.G. Muller, W. Tremel, Adv. Funct. Mater. 21 (2011) 501–509.
[11] W. He, H. Jia, X. Li, Y. Lei, J. Li, H. Zhao, L. Mi, L. Zhang, Z. Zheng, Nanoscale 4 (2012) 3501–3506.
[12] Z. Dai, S. Liu, J. Bao, H. Ju, Chem. Eur. J. 15 (2009) 4321–4326.
[13] S.K. Maji, A.K. Dutta, S. Dutta, D.N. Srivastava, P. Paul, A. Mondala, B. Adhikary, Appl. Catal. B 126–274 (2012) 265.
[14] W. Shi, Q. Wang, Y. Long, Z. Cheng, S. Chen, H. Zheng, Y. Huang, Chem. Commun. 47 (2011) 6695–6697.
[15] Y. Song, K. Qu, C. Zhao, J. Ren, X. Qu, Adv. Mater. 22 (2010) 2206–2210.
[16] Y. Song, X.H. Wang, C. Zhao, K. Qu, J. Ren, X. Qu, Chem. – Eur. J. 16 (2010) 3617–3621.
[17] A. Meidanchi, O. Akhavan, Carbon 69 (2014) 230–238.
[18] J. Lv, B. Li, R. Cao, Chem. Commun. 46 (2010) 8017–8019.
[19] K. Cai, Z. Lv, K. Chen, L. Huang, J. Wang, F. Shao, Y. Wang, H. Han, Chem. Commun. 49 (2013) 6024–6026.
[20] H. Jiang, Z. Chen, H. Cao, Y. Huang, Analyst 137 (2012) 5560–5564.
[21] J. Liu, X. Hu, S. Hou, T. Wen, W. Liu, X. Zhu, X. Wu, Chem. Commun. 47 (2011) 10981–10983.
[22] W. He, X. Wu, J. Liu, X. Hu, S. Hou, K. Zhang, W. Zhou, S. Xie, Chem. Mater. 22 (2010) 2988–2994.
[23] X. Hu, A. Saran, S. Hou, T. Wen, Y. Ji, W. Liu, H. Zhang, W. He, J.-J. Yin, X. Wu, RSC Adv. 3 (2013) 6095–6105.
[24] H. Chen, Y. Li, F. Zhang, G. Zhang, X. Fan, J. Mater. Chem. 21 (2011) 17658–17661.
[25] L. Gao, J. Zhuang, L. Nie, J. Zhang, Y. Zhang, N. Gu, T. Wang, J. Feng, D. Yang, S. Perrett, X. Yan, Nat. Nanotechnol. 2 (2007) 577–583.
[26] K.N. Chaudhari, N.K. Chaudhari, J.-S. Yu, Catal. Sci. Technol. 2 (2012) 119–124.
[27] Y. Chen, H. Cao, W. Shi, H. Liu, Y. Huang, Chem. Commun. 49 (2013) 5013–5015.
[28] M. Liu, R. Zhang, W. Chen, Chem. Rev. 114 (2014) 5117–5160.
[29] N. Li, M. Cao, C. Hu, Nanoscale 4 (2012) 6205–6218.
[30] L.-N. Zhang, H.-H. Deng, F.-L. Lin, X.-W. Xu, S.-H. Weng, A.-L. Liu, X.-H. Lin, X.-H. Xia, W. Chen, Anal. Chem. 86 (2014) 2711–2718.
[31] L. Ai, L. Li, C. Zhang, J. Fu, J. Jiang, Chem. Eur. J. 19 (2013) 15105–15108.
[32] Q. Zhuo, Y. Ma, J. Gao, P. Zhang, Y. Xia, Y. Tian, X. Sun, J. Zhong, X. Sun, Inorg. Chem. 52 (2013) 3141–3147.
[33] H. Woo, J. Park, S. Lee, S. Lee, Chemosphere 97 (2014) 146–152.
[34] Y. Zhang, Y. Su, X. Zhou, C. Dai, A.A. Keller, J. Hazard. Mater. 263 (2013) 685–693.
[35] L. Lu, Z. Ai, J. Li, Z. Zheng, Q. Li, L. Zhang, Cryst. Growth Des. 7 (2007) 459.
[36] T.-F. Yeh, J.-M. Syu, C. Cheng, T.-H. Chang, H. Teng, Adv. Funct. Mater. 20 (2010) 2255–2262.
[37] L. Gu, J. Wang, H.M. Cheng, Y. Zhao, L. Liu, X. Han, ACS Appl. Mater. Interfaces 5 (2013) 3085–3093.
[38] J. Ding, W. Yan, W. Xie, S. Sun, J. Bao, C. Gao, Nanoscale 6 (2014) 2299–2306.
[39] Y.H. Zhang, N. Zhang, Z.R. Tang, Y.J. Xu, ACS Nano 6 (2012) 9777–9789.
[40] A.C. Ferrari, J.C. Meyer, V. Scardaci, C. Casiraghi, M. Lazzeri, F. Mauri, S. Piscanec, D. Jiang, K.S. Novoselov, S. Roth, A.K. Geim, Phys. Rev. Lett. 97 (2006) 187401.
[41] K.N. Kudin, B. Ozbas, H.C. Schniepp, R.K. Prud'homme, I.A. Aksay, R. Car, Nano Lett. 8 (2008) 36–41.
[42] I. Calizo, A.A. Balandin, W. Bao, F. Miao, C.N. Lau, Nano Lett. 7 (2007) 2645–2649.
[43] O. Akhavan, Carbon 81 (2015) 158–166.
[44] K.S. Kim, Y. Zhao, H. Jang, S.Y. Lee, J.M. Kim, K.S. Kim, J.-H. Ahn, P. Kim, J.-Y. Choi, B.H. Hong, Nature 457 (2009) 706–710.
[45] Z. Ai, Z. Gao, L. Zhang, W. He, J.J. Yin, Environ. Sci. Technol. 47 (2013) 5344–5352.
[46] F.-X. Xiao, J. Miao, B. Liu, J. Am. Chem. Soc. 136 (2014) 1559–1569.
[47] Y. Min, G. He, Q. Xu, Y. Chen, J. Mater. Chem. A 2 (2014) 1294–1301.
[48] L. Su, J. Feng, X.M. Zhou, C.L. Ren, H.H. Li, X.G. Chen, Anal. Chem. 84 (2012) 5753–5758.
[49] N. Li, Y. Yan, B.-Y. Xia, J.-Y. Wang, X. Wang, Biosens. Bioelectron. 54 (2014) 521–527.
[50] L. Li, L. Ai, C. Zhang, J. Jiang, Nanoscale 6 (2014) 4627–4634.
[51] R.C.C. Costa, F.C.C. Moura, J.D. Ardisson, J.D. Fabris, R.M. Lago, Appl. Catal. B 83 (2008) 131–139.
[52] X. Lv, X. Xue, G. Jiang, D. Wu, T. Sheng, H. Zhou, X. Xu, J. Colloid Interface Sci. 417 (2014) 51–59.